

Article

# 3D-printed poly (lactic acid) scaffolds coated with cationic macro-biocide: Investigation of anti-biofilm activity and thermo-mechanical properties

Figen Aynali<sup>1,\*</sup>, Gizem Urtekin<sup>2</sup>, Levent Aydın<sup>3</sup>, Huseyin Balci<sup>4</sup>, Metin Cetin<sup>4</sup>, Guralp Ozkoc<sup>5,\*</sup>

<sup>1</sup> Department of Chemical Engineering, Gebze Technical University, Kocaeli 41400, Turkey

<sup>2</sup> Department of Chemical Engineering, Kocaeli University, Kocaeli 41380, Turkey

<sup>3</sup> Department of Podiatry, Kocaeli University, Kocaeli 41380, Turkey

<sup>4</sup> Department of Molecular Biology and Genetics, Gebze Technical University, Kocaeli 41400, Turkey

<sup>5</sup> Department of Chemistry, Istinye University, Istanbul 34010, Turkey

\* **Corresponding authors:** Figen Aynali, [figenaynali@gmail.com](mailto:figenaynali@gmail.com); Guralp Ozkoc, [guralp.ozkoc@istinye.edu.tr](mailto:guralp.ozkoc@istinye.edu.tr)

## CITATION

Aynali F, Urtekin G, Aydın L, et al. 3D-printed poly (lactic acid) scaffolds coated with cationic macro-biocide: Investigation of anti-biofilm activity and thermo-mechanical properties. *Materials Technology Reports*. 2025; 3(1): 1400. <https://doi.org/10.59400/mtr1400>

## ARTICLE INFO

Received: 18 November 2024

Accepted: 25 January 2025

Available online: 3 March 2025

## COPYRIGHT



Copyright © 2025 by author(s). *Materials Technology Reports* is published by Academic Publishing Pte. Ltd. This work is licensed under the Creative Commons Attribution (CC BY) license. <https://creativecommons.org/licenses/by/4.0/>

**Abstract:** In this study, the primary goal was to combine surface modification and 3D printing technology to create materials with anti-biofilm action. In order to achieve this, first a two-step reaction procedure using ring-opening copolymerization and copper(I)-catalyzed azide-alkyne cycloaddition click reaction was used to successfully fabricate poly (lactic acid) (PLA) bearing quaternary ammonium salt (QAS) as an antimicrobial agent on its backbone at rates of 5% by mole. Then, this synthesized PLA-based (co)polymer dissolved in acetone with a weight percentage of 30% was used to coat 3D-printed PLA by dipping for 10, 30, and 90 s. These coated samples encoded PLA/10/PLA-QAS, PLA/30/PLA-QAS, and PLA/90/PLA-QAS, respectively. The coated PLA scaffolds were then characterized by Fourier transform infrared spectroscopy (FT-IR) and scanning electron microscopy (SEM). Gram-positive (*Staphylococcus aureus*) and Gram-negative (*Escherichia coli*) bacteria were used to assess the anti-biofilm activity of the samples. In addition, the thermal and mechanical properties of the samples were examined through differential scanning calorimetry (DSC) and three-point bending tests, respectively. Consequently, covering the 3D-printed PLA surfaces with synthesized antimicrobial polymer prevented the formation of biofilms against both bacteria, and all coated samples showed no toxicity in 25% and 10% extraction mediums. And, it was observed that the antimicrobial polymer solution had a plasticizing effect on the PLA scaffold. As the dipping times increased, the glass transition temperatures of the coated samples decreased. In terms of flexural behaviors, increasing the dipping time also improved the flexural strain of coated PLA scaffolds. These thermo-mechanical results are correlated with SEM morphologies because of the penetration and solution effect of antimicrobial polymer dissolved in acetone.

**Keywords:** 3D printing; poly (lactic acid); quaternary ammonium salt; surface modification; biofilm activity

## 1. Introduction

Three-dimensional (3D) printing, often known as additive manufacturing (AM), is widely regarded as a revolutionary manufacturing technology of the twenty-first century [1–3]. Due to advancements over the previous ten years, 3D printing has the potential to replace several traditional subtractive manufacturing technologies. By enabling the quick and affordable fabrication of such unique goods that cannot be made using traditional manufacturing processes like injection molding for implants and tableting for oral drug dosage forms, 3D printing has found its place in nanotechnology, medicine, and tissue engineering [4–7]. Nowadays, the use of 3D

printing to improve bioengineered tissues and blood vessels, as well as to produce useful biomedical materials and devices for orthopedic and dental applications, is the subject of extensive research [8].

Poly (lactic acid) (PLA), polyetheretherketone (PEEK), polycarbonate (PC), and other materials can now be used as 3D filament materials. Despite this variability, PLA printing is currently the preferred option for many applications [7,9]. The Food and Drug Administration (FDA) has approved the use of PLA, a thermostable aliphatic polyester made from a monomer derived from sugarcane, sugar beet, corn, and cassava, for use in human applications. Because of its biodegradability, biocompatibility, superior mechanical strength, and processability, it is an ideal polymer for *in vivo* applications. One of the most important advantages of PLA over non-degradable biomaterials is that the implant can be removed without extra surgery. In addition, PLA's poor conductivity prevents it from causing an electrochemical reaction in the body. In conclusion, it is a key biomaterial with a variety of uses in both industry and medicine [10–12]. Unfortunately, there are considerable limitations for many applications of PLA due to the absence of reactive side-chain groups, which makes it extremely difficult to modify surfaces [13]. Plasma therapy, photografting, or wet chemistry have all significantly improved the ability to permanently modify surfaces [14–18]. However, due to the degrading conditions of PLA, they all have certain issues. Therefore, it is essential to develop a simple method for functionalizing PLA's surface and enabling the immobilization of a wide range of bioactive chemicals. This procedure should: (i) prevent polymer degradation; and (ii) offer an activated stable surface that can be altered by a simple procedure for the addition of small molecules, biomolecules, and macromolecules without altering the properties of these active compounds. These criteria are satisfied by click chemistry, particularly the Cu(I)-catalyzed Huisgen 1,3-dipolar cycloaddition of alkynes and azides (CuAAC). Because click chemistry is a successful technique that may be used in mild experimental conditions and produces high yields [19–22].

Biofilms may result in material damage because the secretion of implanted cells can degrade most synthetic materials. These risks have put people's health in danger and can even cause human deaths [23]. The development of bulk materials with antimicrobial properties is currently receiving close scientific attention, notably for a variety of applications in the health sector that aim to improve environmental cleanliness and stop the spread of illnesses caused by pathogenic microbes [24–26]. Many bulk 3D objects made of polymers, a large family of plastic materials used in a variety of applications including hospital tables, paints, protective equipment, and biomedical products like bandages, implants, surgery equipment, catheters, etc., have been modified by antimicrobial agents using solvent mixing or melt-mixing techniques. Additionally, another beneficial method to bring the antibacterial property to bulk 3D plastic components is depositing antimicrobial films onto their outer surface by (i) either wet chemical methods (dip-coating using AgNP dispersions, sonochemical immobilization, etc.) or (ii) vacuum deposition techniques (magnetron sputtering, ion-beam-assisted deposition process, etc.) [27,28].

It is known that there may be some unknown risks associated with coating implant surfaces with low molecular weight antimicrobial agents due to toxicity to human body, residues, and the short action duration that results in polluted surfaces

again after being exposed to pathogens [29–31]. Another option is to coat the implant surfaces with a thin film of a contact-active antibacterial polymer that contains an agent to prevent microbial infections. Typically, quaternary ammonium salts that are covalently linked to a polymeric chain or substrate offers the contact active (or contact killing) action [32–34]. These cationic macro-biocides find application in diverse daily objects such as doorknobs, kid’s toys, computer keyboards, phones, paints for hospital rooms, and biomedical equipment like bone screws, catheters, and surgical sutures, among others. Additionally, they can be utilized in food packaging to maintain quality until the ultimate customer is reached and in the textile business to produce antimicrobial fibers [35,36]. Because they address the aforementioned issues, contact-active antimicrobial surfaces have garnered a lot of attention in recent years.

Recently, the use of antimicrobial PLA materials has become widely recognized for its ability to solve the problem of bacterial contamination and the development of biofilms on medical equipment and other relevant fields. This can be accomplished using the dip-coating method, which involves submerging the device into an antimicrobial solution. This process results in the creation of a thin protective layer on the device that provides extended and effective antimicrobial protection. A crucial area where 3D printed PLA materials with anti- biofilm properties can be utilized is in the realm of surgical instruments. These instruments often become contaminated with bacteria, leading to the possibility of infections and negative outcomes for patients. By using the dip-coating method to apply antimicrobial PLA coatings, the growth of bacteria on the surface of the instruments can be inhibited, thus lowering the risk of infection. This not only improves overall sterilization but also decreases the chance of transmitting harmful microorganisms during surgical procedures. Another application of 3D printed PLA materials with anti-biofilm properties can be seen in medical implants, like artificial joints and heart valves. By coating the implants with antimicrobial PLA, it can stop the development of harmful microorganisms, reducing the likelihood of infections and other adverse effects on patients. Additionally, the anti-biofilm feature of the coating can enhance the durability and performance of the implant, as biofilm formation can affect the implant’s functioning. Wound dressings can benefit greatly from 3D printed PLA materials with anti-bacterial properties. Bacterial contamination can impede the healing process of wounds and increase the chance of infections. By using the dip-coating method to apply an antimicrobial PLA coating to the surface of the dressings, the growth of bacteria can be prevented, leading to quicker healing and reducing the risk of infections. Catheter usage in medical procedures is another area where 3D printed PLA materials with anti-bacterial properties can make a noticeable difference. Catheter-related infections are a common concern in the medical field. By applying antimicrobial PLA coatings through the dip-coating process, the risk of infections can be lowered by hindering the growth of bacteria on the catheter’s surface. This can enhance overall patient outcomes and decrease the transmission of harmful microorganisms. Finally, the anti-biofilm properties of 3D printed PLA materials can also be utilized on hospital surfaces, including bedrails and equipment. These surfaces are often contaminated with bacteria, which can cause the spread of infections and put patients and healthcare workers at risk. By applying antimicrobial PLA coatings using the dip-coating method,

the spread of infectious diseases can be prevented and overall hygiene in the hospital environment can be improved [37–40].

The primary goal of this work was to create 3D-printed materials with anti-biofilm properties due to covalently linked antimicrobial compounds. In order to do this, quaternary ammonium salt was bonded to the PLA copolymer by click chemistry at a rate of 5 mole%. After obtaining the antimicrobial polymer, it was employed to coat the 3D-printed PLA surfaces via the dip-coating method by applying three different waiting times. Using the contact-active approach, the antibacterial activity of all coated samples was tested against Gram-negative (*Escherichia coli*) and Gram-positive (*Staphylococcus aureus*) bacteria. Using differential scanning calorimetry (DSC), the thermal properties of the films were investigated. Additionally, three-point bend testing was used to examine how the dip-coating process affected the mechanical properties. In addition, a cytotoxicity test was carried out. In summary, it was possible to create anti-biofilm active surfaces with tolerable cytotoxicity without significantly altering the mechanical characteristics of the 3D-printed PLA scaffolds.

## 2. Experimental

### 2.1. Materials

For synthesis, (3S)-cis-3,6-dimethyl-1,4-dioxane-2,5-dione (LA) (Aldrich, Steinheim, Germany, 98%) was purified by recrystallization three times from dry toluene. Tin(II) 2-ethylhexanoate (Sn(Oct)<sub>2</sub>) (Aldrich, 95%), N,N-dimethylprop-2-yn-1-amine (Sigma-Aldrich Steinheim, Germany, 97%), sodium azide (NaN<sub>3</sub>) (Sigma-Aldrich, 99.5%), 2,2-bis(bromomethyl)-1, 3-propanediol (Sigma-Aldrich, 98%), 1-bromododecane (Alfa Aesar, Haverhill, Massachusetts, USA, 98%), dodecanol (Sigma-Aldrich, 98%), copper(II) sulfate pentahydrate and sodium ascorbate were used as purchased without further purification. Triethylamine (TEA) ( $\geq 99.5\%$ ) was obtained from Sigma-Aldrich, dried over CaH<sub>2</sub> and stored over 3 Å molecular sieves. The PLA filament used in this study was a non-medical grade, environment-friendly material, obtained as a consumable product from Rhino3D, a supplier based in Istanbul. This material was manufactured by Esun Industrial Co., Ltd., Shenzhen, China, and is commercially available. PLA exhibits mechanical and physical properties that make it a popular choice for various industries, including food packaging, textiles, and consumer goods. With a density of 1.24 g/cm<sup>3</sup>, it ensures consistent dimensional stability during printing. The filament offers a tensile strength of 65 MPa and a flexural strength of 74 MPa, highlighting its robustness and resistance to deformation. Its flexural modulus, measured at 1973 MPa, ensures rigidity, while an elongation at break of 20% provides moderate flexibility for intricate designs. The material also features intrinsic viscosity values ranging from 0.61 to 8.2 dL/g, indicating high molecular weight and thermal stability, which contribute to smooth extrusion and minimal warping during fabrication [41].

### 2.2. Synthesis of antimicrobial copolymers having antimicrobial agents bound via covalent bond

Firstly, quaternary ammonium salt substituted by the dodecyl group (N, N-

dimethyl-*N*-prop-2-yn-1-yl-dodecane-1-ammonium bromide, QAS-12C) was synthesized. Then, this synthesized antimicrobial agent was introduced into azido-functionalized copolymers at a rate of 5 mole% via click chemistry to obtain (P(LA<sub>0.95</sub>-co-ADTC<sub>0.05</sub>-QAS-12C, PLA-QAS)). All synthesis methods were explained in detail in previously published synthesis work [42]. The general reaction mechanism was also shown in **Figure 1**.

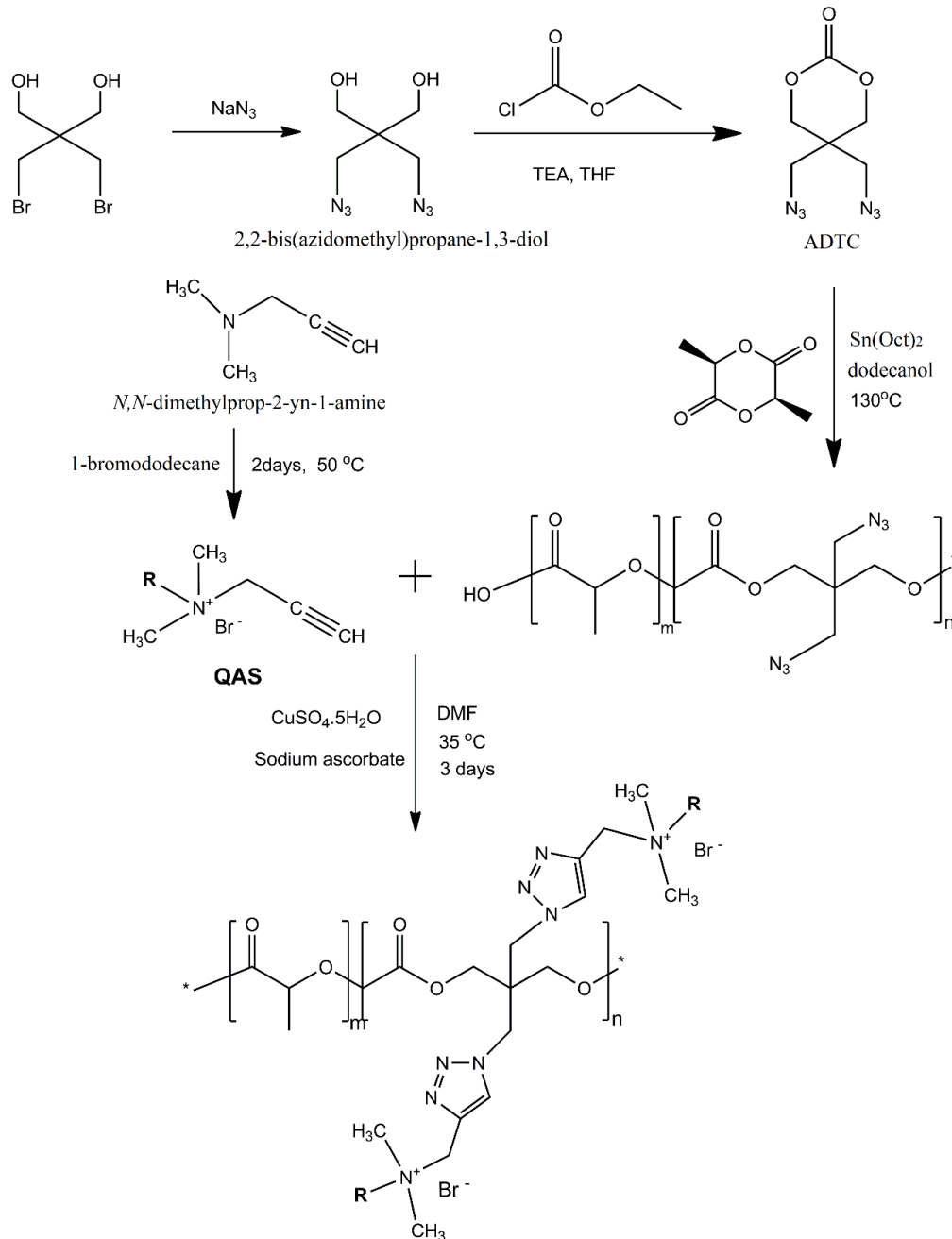


**Figure 1.** General reaction mechanism to obtain P(LA<sub>0.95</sub>-co-ADTC<sub>0.05</sub>-QAS-12C) encoded as PLA-QAS (R ≡ –C<sub>12</sub>H<sub>25</sub>; *m/n*: 0.95/0.05).

### 2.3. Preparation of 3D printed scaffold

Test specimens were first modeled and exported as a Standard Tessellation Language file (STL) in Solidworks 2016 (Dassault Systèmes) workspace based on

ISO (International Standard of Organization) 178, which is an applicable standard for additively manufactured objects as mentioned in the National Institute of Standards and Technology (NIST) report [43]. Then, a Fused Deposition Modeling (FDM) method-based additive manufacturing system (Ender 3 Pro, Creality) was used to produce test specimens. Before the printing stage, path planning was provided via Ultimaker Cura slicer software with predetermined parameters as given in **Table 1**. During the printing stage, a PLA filament (Porima) was used to create the series of successive layers and finally, each specimen was analyzed.

**Table 1.** Slicing parameters of test specimens.

Parameter	Value
Layer height (mm)	0.15
Line width (mm)	0.4
Wall thickness (mm)	0.4
Top/bottom pattern	Lines
Infill (%)	100
Infill pattern	Lines
Printing temperature (°C)	210
Build plate temperature (°C)	60
Flow (%)	100
Retraction	Enabled
Print speed (mm/s)	60
Print cooling	Enabled
Support	Disabled
Build plate adhesion	Disabled

#### 2.4. Surface coating of PLA scaffolds with synthesized antimicrobial polymer

The surface modifications of the PLA scaffolds were carried out using the direct absorption of synthesized antimicrobial PLA-based copolymer (PLA-QAS) onto the 3D-printed PLA scaffold. For the coating process, a solution with a weight percentage of 30% for synthesized PLA-QAS was first prepared in acetone with magnetic stirring. The PLA-QAS solution was coated onto the surface of PLA scaffolds using the dip coating method [44]. Samples were kept in the prepared solution for 10, 30, and 90 seconds, and the process was repeated five times for each parameter. All samples were dried in a fume hood for one day. The schematic illustration of fabricating 3D-printed PLA coated with an antimicrobial polymer was given in **Figure 2**. The prepared films were encoded as PLA/10/PLA-QAS, PLA/30/PLA-QAS, and PLA/90/PLA-QAS for each waiting time.

#### 2.5. Fourier transform infrared (FTIR) analysis

The samples were subjected to attenuated total reflectance Fourier transform infrared spectroscopy (ATR FTIR) using a Paragon 1000 spectrometer (Perkin Elmer, USA) fitted with a single-reflection device, the PIKE MIRacle™ diamond (Pike

Technologies, Madison). At room temperature, the data was collected with a spectral resolution of  $4\text{ cm}^{-1}$ , covering a frequency range of  $650\text{ to }4000\text{ cm}^{-1}$ .

## 2.6. Scanning electron microscopy (SEM)

The morphological monitoring of the surfaces was characterized by using SEM (Philips XL30 FEG, Oregon, USA). Since all samples were prepared under the same conditions, only one sample in each experimental series was analyzed.

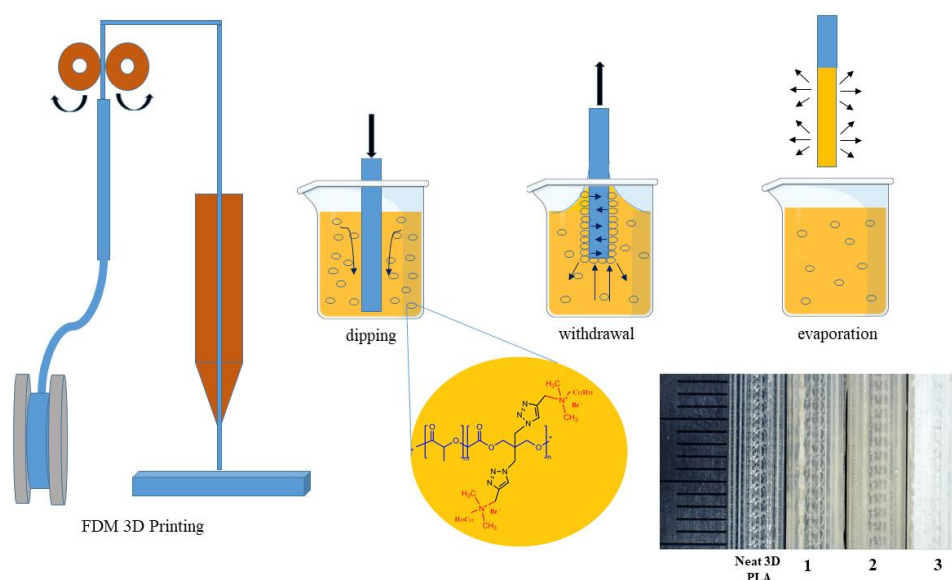


**Figure 2.** Schematic illustration of fabricating 3D printed PLA coated with an antimicrobial polymer (1: PLA/10/PLA-QAS; 2: PLA/30/PLA-QAS, and 3: PLA/90/PLA-QAS).

## 2.7. Assessment of anti-biofilm activity of the coated scaffolds

Gram-positive *Staphylococcus aureus* (ATCC 29213) and Gram-negative *Escherichia coli* (ATCC 53323) were used to test the anti-biofilm activity. Three pieces of  $1\text{ cm} \times 1\text{ cm}$  were cut from each PLA sample (PLA/10/PLA-QAS, PLA/30/PLA-QAS, and PLA/90/PLA-QAS) and sterilized with 70% ethanol. After being dried in the laminar flow, they were aseptically transferred to sterile 24-well plates, with each well holding a 2-milliliter bacterial suspension of either *S. aureus* or *E. coli* at a final concentration of  $10^5\text{ CFU mL}^{-1}$  in the suitable growth conditions (Tryptic Soy Broth and Tryptic Soy Broth 66% supplemented with glucose 0.2% for *E. coli* and *S. aureus*, respectively). Plates were then incubated under static conditions for 48 h at  $37\text{ }^\circ\text{C}$  in a 100% humidity atmosphere to allow the formation of biofilms. For control, uncoated PLA scaffolds were used. After biofilms grew on the samples, they were carefully washed three times with distilled water to remove any non-adherent cells. They were then carefully transferred to new 24-well plates and the biofilms were quantified using the crystal violet assay as previously described with minor modifications [44]. The membranes were stained with 0.4% crystal violet ( $500\text{ }\mu\text{L}$ ) at room temperature for 15 min. Unbound and excess dye was removed by careful washing with distilled water three times, and the samples were carefully transferred into new 24-well plates. Crystal violet retained by the biofilm was dissolved in 500

$\mu\text{L}$  of 33% acetic acid for 15 min, and absorbance was determined at 550 nm using the Fluostar Omega Microplate Reader (BMG Labtech, Ortenberg, Germany).

## 2.8. Three-point bending test

Three-point bending tests were made with the Universal Testing Machine LRX Plus series motorized test stand on the Lloyd instrument. The test was planned according to ASTM D790 using NEXYGEN™ data analysis software to determine the flexural properties of samples. The samples were performed at a crosshead displacement of 4 mm/min with a 5 kN load cell at room temperature. The length of the support span is 67 mm. 3 parallel tests were operated for each sample. In **Figure 3**, a test example was displayed. The machine extension is limited to 20 mm in all samples and the test ended after the 20 mm extension. The thickness and width were measured for each sample before the test was entered into the program. The width and thickness of the samples were approximately 4.15 mm and 1.75 mm.

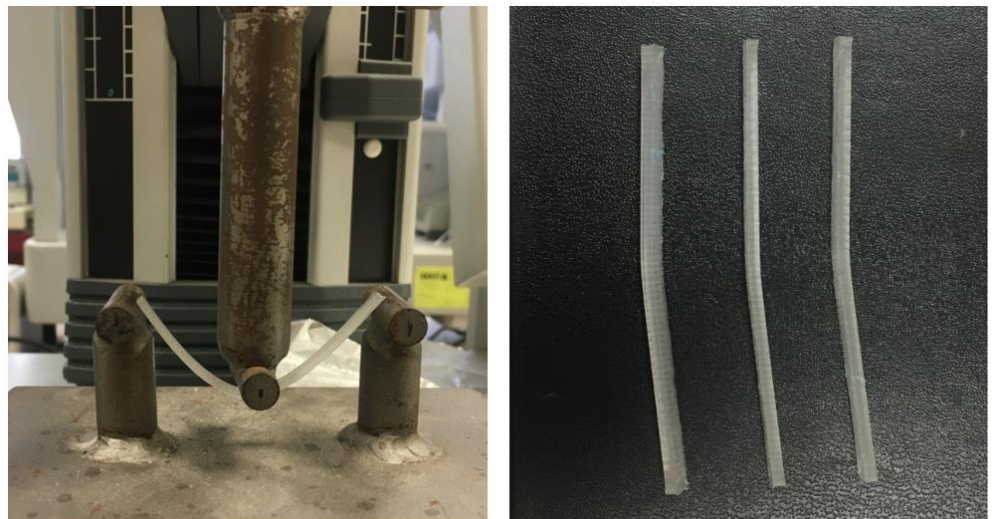


**Figure 3.** Three-point bending test for PLA/90/PLA-QAS sample.

## 2.9. The differential scanning calorimetry analysis

The analysis of the thermal properties of samples was carried out using a Mettler Toledo DSC. The thermal transitions, such as glass transition temperature, melting, and cold crystallization of the samples, were determined and plotted on the graph of heat flow versus temperature. The rate of 1st heating/cooling/2nd heating was  $10\text{ }^{\circ}\text{C min}^{-1}$  between room temperature and  $200\text{ }^{\circ}\text{C}$ . Experiments were applied under an inert nitrogen atmosphere ( $\text{N}_2$ ) using an alumina crucible.

## 2.10. Indirect cytotoxicity and cell viability assay

Cytotoxicity was assessed in vitro using a slightly modified version of the ISO 10,993-5 extraction procedure [45]. In summary, the samples underwent a 30-min UV sterilization step prior to being submerged in five milliliters of complete media (DMEM High Glucose, Gibco, USA), 10% FBS (Gibco, USA), 1% Penn/Strep (Gibco, USA), and 1% Non-essential Amino Acid (NEAA) (Gibco, USA). The samples were then incubated for seventy-two hours at  $37\text{ }^{\circ}\text{C}$  and 5%  $\text{CO}_2$ . Then, a 0.22

$\mu\text{M}$  filter was used to collect and filter the extraction media. HuH7 Hepatocellular Carcinoma was used to examine the extraction medium's effect on cell viability after it was collected from samples. Crystal Violet (CV) Staining is an assay that uses colony formation to analyze cell lines [46]. HuH7 cells ( $1 \times 10^4$ ) were seeded in triplicate in a 24-well plate. After the cells were attached and found to have morphology, extraction mediums of control (only DMEM, 0%), PLA/10/PLA-QAS, PLA/30/PLA-QAS, and PLA/90/PLA-QAS were diluted to 50%, 25%, and 10% with fresh complete media and treated for 48 h. After the treatment, cells were washed twice with phosphate buffered saline (PBS) and fixed with formaldehyde (4%, 20 min at room temperature). After the fixation, cells were washed twice with PBS and incubated with the 1% crystal violet (CV) solution for 10 min at room temperature. After a gentle PBS wash, the cells were dried upside down. To quantify the wells, 200  $\mu\text{L}$  of 10% methanol, 10% acetic acid, and 80% water were added to CV and agitated for 10 min. Then, 100  $\mu\text{L}$  from each well was transferred to a 96-well plate, and the optical densities (OD) of the wells were measured at 590 nm using a Varioscan Microplate reader (Thermo Scientific, Waltham, MA, USA). When compared to DMEM-only control cells, the average OD values were then translated to % Cell Viability. More than 70% vitality is regarded by ISO standards as non-toxic and cyto-compatible.

### 3. Results and discussion

#### 3.1. FT-IR spectroscopy analysis

FT-IR spectroscopy was used to look for any potential interactions. **Figure 4** demonstrates the spectrum of synthesized polymer and 3D-printed sample exposed to the antimicrobial solution for 90 s via dip-coating (PLA/90/PLA-QAS). In **Figure 4** for both spectrums, the C-H stretching vibrations of the  $\text{CH}_2$  and  $-\text{CH}_3$  groups can be identified as two signals at 2925 and 2860  $\text{cm}^{-1}$ , respectively, while the bending C-H vibrations of the  $-\text{CH}_2$  and  $-\text{CH}_3$  groups can be seen at 1461 and 1384  $\text{cm}^{-1}$ . The most intense signal at 1726  $\text{cm}^{-1}$  was the stretching vibration peak of  $\text{C}=\text{O}$ . These all signals belong to neat PLA and in addition to these, the clear characteristic  $-\text{NH}$  at 3543  $\text{cm}^{-1}$  and unsaturated triazole ring vibration bands at 1608  $\text{cm}^{-1}$  were seen for the synthesized PLA based antimicrobial polymer in **Figure 4a**. This circumstance demonstrates that QAS attached to the polymer backbone via click reaction. In **Figure 4b**, in addition to the expected neat PLA signals, the same distinctive signals at 1608  $\text{cm}^{-1}$  that correspond to the triazole ring give qualitative evidence for the presence of antimicrobial polymer on the 3D-printed PLA sample. Furthermore, the lack of additional absorption bands indicates that the coating is not causing any chemical reactions.

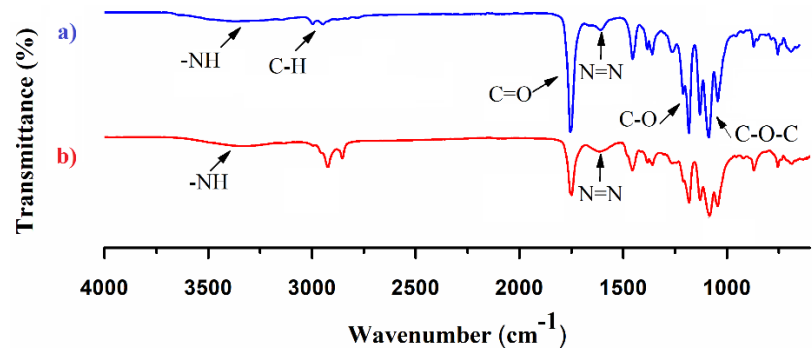
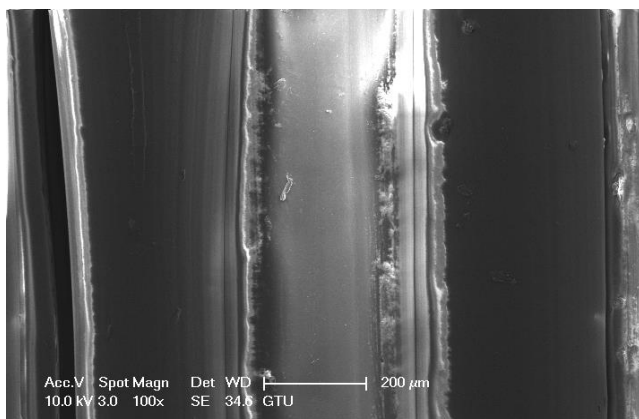


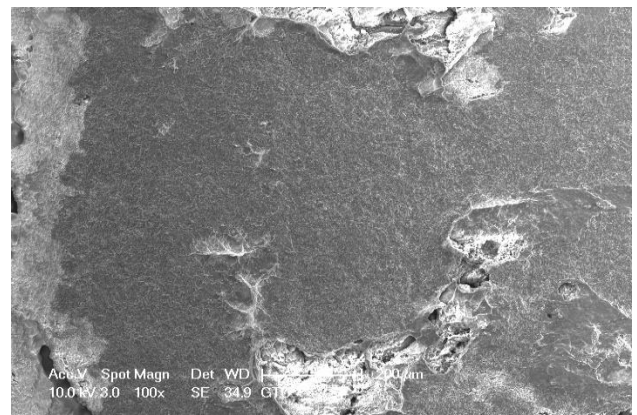
**Figure 4.** FTIR spectra of: (a) PLA-QAS; (b) PLA/90/PLA-QAS.

### 3.2. Scanning electron microscopy analysis

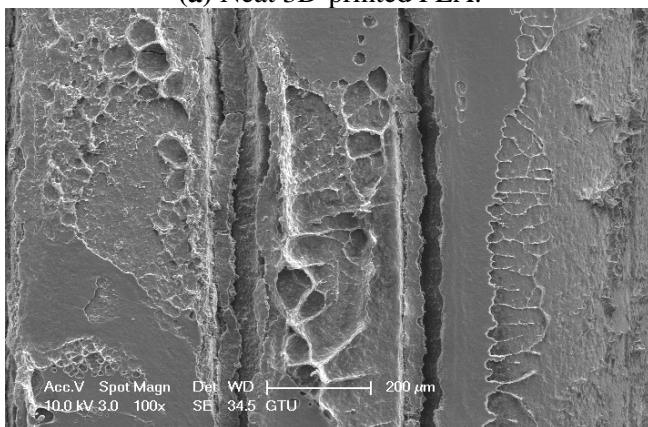
**Figures 5 and 6** displayed the SEM microphotographs of neat and coated 3D-printed PLA samples. SEM micrographs of each sample with a scale bar of 200 microns are shown in **Figure 5**. It displays how the surface of samples was changed after being exposed to antimicrobial polymer in acetone. When exposed to antimicrobial polymer solution for 10 and 30 s, a crystallization effect was seen on the surface of scaffolds (**Figure 5b,c**). But while increasing the exposure time, the crystals could not be seen due to dissolution of the PLA scaffold (**Figure 5d**).



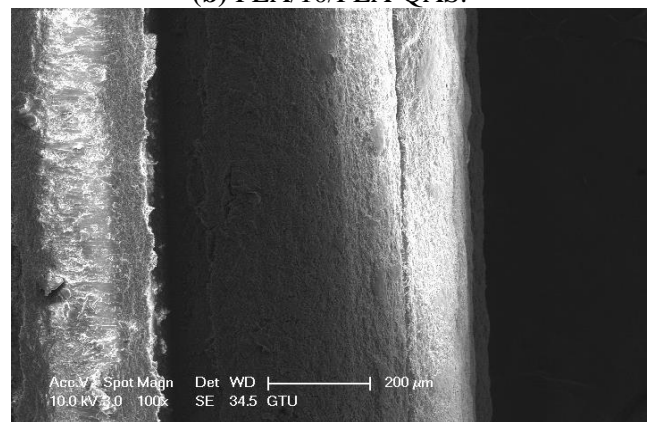
**(a)** Neat 3D-printed PLA.



**(b)** PLA/10/PLA-QAS.



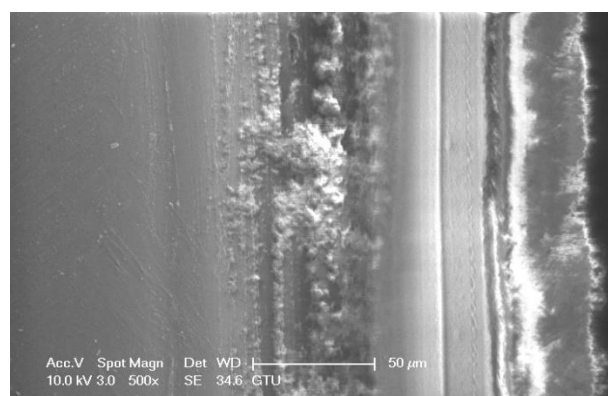
**(c)** PLA/30/PLA-QAS.



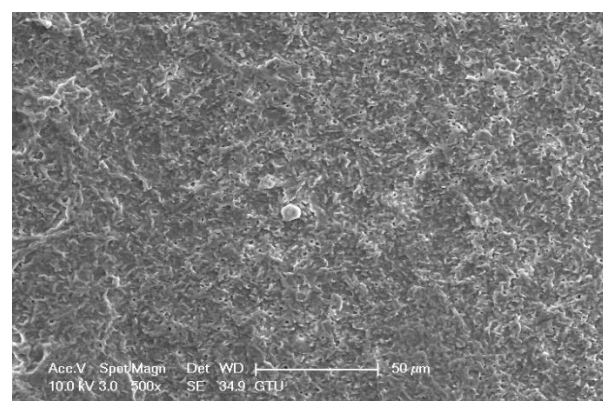
**(d)** PLA/90/PLA-QAS.

**Figure 5.** SEM micrographs of neat and coated 3D printed PLA based scaffolds (Magnification: X100, scale bar: 200 microns).

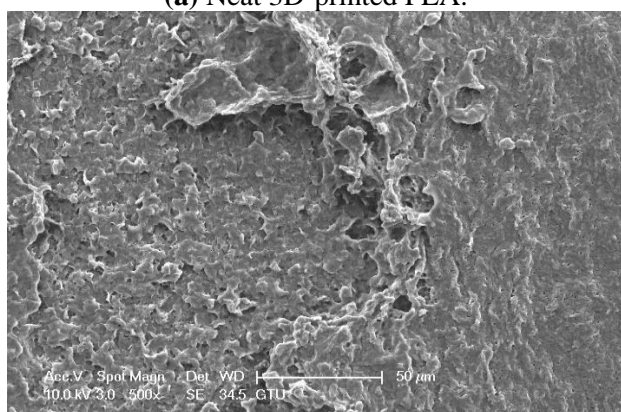
In addition, the SEM microphotographs of all scaffolds were shown in **Figure 6** at a 50-micron scale bar. It is more clearly seen that structural changes have occurred on the surfaces of the PLA/10/PLA-QAS (**Figure 6b**) and PLA/30/PLA-QAS (**Figure 6c**) samples due to the penetration of antimicrobial polymer solution prepared using acetone as a solvent. As stated before, the effect of the polymer solution on dissolving the PLA scaffold is seen more clearly in **Figure 6d** (PLA/90/PLA-QAS).



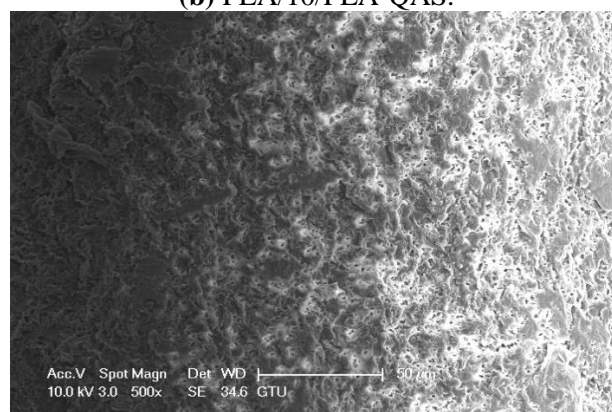
(a) Neat 3D-printed PLA.



(b) PLA/10/PLA-QAS.



(c) PLA/30/PLA-QAS.



(d) PLA/90/PLA-QAS.

**Figure 6.** SEM micrographs of neat PLA and all films coated with P1 (Magnification: X500, scale bar: 50 microns).

### 3.3. Antimicrobial activity

Biofilm formation was evaluated by quantitative analysis using the crystal violet method. Anti-biofilm activity was found in both bacterial strains tested. **Figure 7** shows that biofilm formation was inhibited by coating the 3D-printed PLA surfaces with antimicrobial polymer. About a 70% reduction in OD600 was achieved with all three coated samples for *S. aureus* compared to the control neat PLA scaffold. Similarly, *E. coli* biofilms were inhibited by 55%, 60%, and 70% on PLA/10/PLA-QAS, PLA/30/PLA-QAS, and PLA/90/PLA-QAS, respectively, compared to the control neat 3D printed PLA.

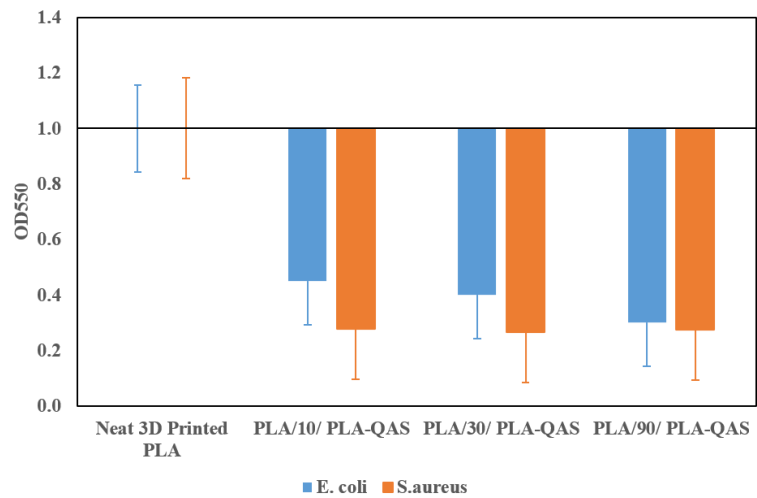


**Figure 7.** Quantification of biofilms on surfaces of scaffolds after 48 h by crystal violet staining and measurement of released stained bacteria at OD 550. results are expressed relative to biofilm on control 3D-printed PLA (data are given as means  $\pm$  SD and correspond to measurements in triplicate).

### 3.4. Three-point bending test

The flexural behaviors of the uncoated neat 3D-printed PLA and all coated samples were characterized by the three-point bending test. Load–extension curves were shown in **Figure 8** for all samples. The uncoated PLA scaffold demonstrated the highest flexural properties among the samples. As can be seen from **Table 2**, the neat PLA scaffold demonstrated the highest flexural strength and modulus. The flexural stress and flexural strain were recorded at 80.3 MPa and 0.03 mm/mm, respectively, in the bending test result, as in agreement with previously published data [47]. Also, it was observed that as the waiting time in the antimicrobial solution increased, the stress and modulus of the coated PLA scaffolds decreased.

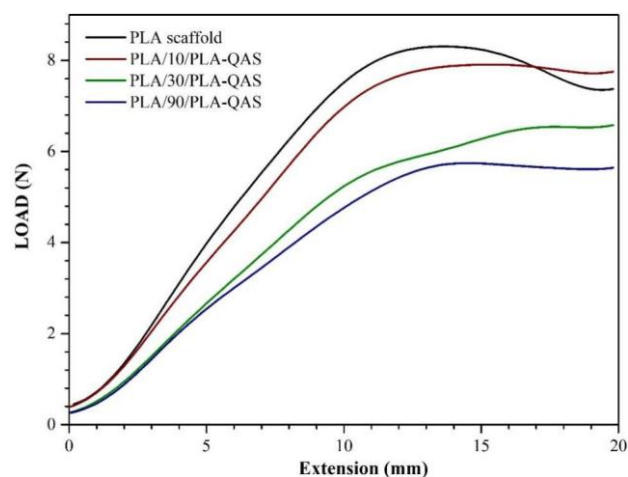


**Figure 8.** Load versus extension curves of samples after three-point bending test.

**Table 2.** The flexural behaviors of the PLA scaffolds.

Sample codes	Flexural Stress (MPa)	Flexural Strain (mm/mm)	Flexural Modulus (MPa)
3D printed PLA	84.6	0.030	10,574
PLA/10/PLA-QAS	59.5	0.034	4400
PLA/30/PLA-QAS	53.3	0.044	3301
PLA/90/PLA-QAS	43.1	0.046	3292

When focusing on the bending strain, it was observed that the situation was the opposite. The highest flexural strain belonged to PLA/90/PLA-QAS. Increasing the dipping time improved the antimicrobial polymer dissolved in acetone, which penetrated the coated PLA scaffolds, and the flexural strain improved with longer dipping times. This result is correlated with the SEM micrographs.

### 3.5. Differential scanning calorimetry analysis

DSC was performed to investigate the temperature behavior of the neat and all coated 3D-printed PLA samples. Multiphase transitions involving a glass transition, cold crystallization, and melting were recorded as given in **Table 3**. The glass transition temperature of the neat PLA scaffold was marked at 60.2 °C. A reduction was observed in the  $T_g$  of the coated samples compared to the neat PLA scaffold. The lowest glass transition temperature of 53 °C belongs to the PLA/90/PLA-QAS. It has been observed that the antimicrobial polymer solution has a plasticizing effect on the PLA scaffold. As the dipping times increased, the plasticizing effect increased, and the glass transition temperatures of the coated samples decreased. While PLA/10/PLA-QAS and PLA/30/PLA-QAS gave approximately the same melting temperatures ( $T_m$ ) with the neat 3D-printed PLA sample, the  $T_m$  of PLA/90/PLA-QAS dropped by 5 °C. Likewise, it has been found that the longer the dipping time, the lower the melting temperatures. Finally, it can be said that these results are expected by looking at the SEM micrographs and correlated with the three-point bending test.

**Table 3.** Thermal properties of samples by DSC.

Sample codes	$T_g$ (°C)	$T_{cc}$ (°C)	$T_m$ (°C)
PLA	60.2	127	151.5
PLA/10/PLA-QAS	58	126	150.4
PLA/30/PLA-QAS	54.5	130.2	149
PLA/90/PLA-QAS	53	116	145.6

### 3.6. Cytotoxicity

Extraction mediums of all samples were further diluted with complete media to obtain 50%, 25%, and 10% extraction mediums and cells were treated for 48 h with these diluted extraction mediums. The viability of the cells was assessed through the colony formation ability under the treatment. The emerged colonies after 48 h later were stained with crystal violet and dissolved with a methanol: acetic acid: water (10%:10%:80%) mixture. %Cell viability was calculated based on the OD values of only DMEM control (**Figure 9**). The reference uncoated control scaffold showed no toxicity at given extraction mediums whereas all coated samples showed around 20%

cell viability in 50% extraction mediums after the incubation. On the other hand, they were not toxic in the other two concentrations, considering the safety threshold below 70% viability according to ISO norms.

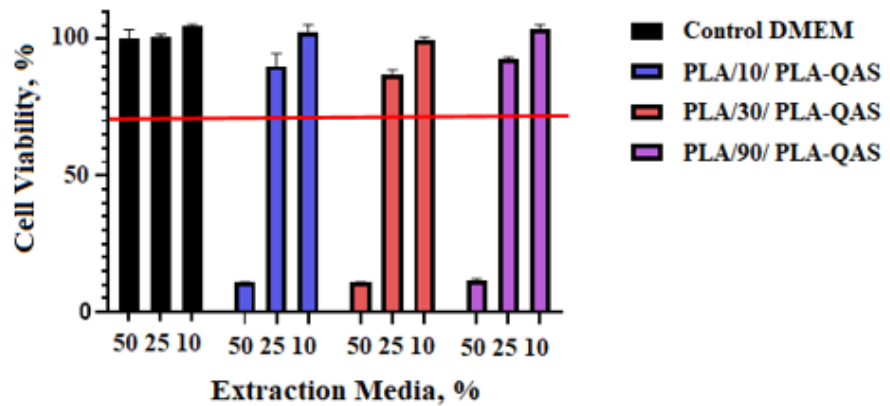


**Figure 9.** Indirect cytotoxicity of the extraction mediums. HuH7 cells were stained with crystal violet after treatment of all samples in various concentrations. After the solubilization of crystal violet in each well, OD was read at 590 by Varioscan microplate reader (Lower panel).

#### 4. Conclusion

In this study, 3D-printed materials have anti-biofilm activity by antimicrobial agents bound by covalent bonds. To do this, quaternary ammonium salt was initially added by click chemistry at a rate of 5 mole% to the PLA copolymer's backbone. Then, 3D-printed PLA scaffolds were coated via the dip-coating method by waiting for 10, 30, and 90 s in the antimicrobial polymer solution. The presence of antimicrobial PLA-based copolymer on the neat 3D-printed PLA scaffold was determined by FTIR analysis by showing the clear characteristic -NH at 3543  $\text{cm}^{-1}$  and unsaturated triazole ring vibration bands at 1608  $\text{cm}^{-1}$ . In addition, scanning electron microscopy was used for morphological monitoring of the surfaces. It was found that the surfaces of the 3D-printed PLA samples crystallized after the 10 and 30 s dip-coating processes. However, the coating method lost its crystallization impact on the samples as the coating time increased because of the dissolution effect of the antimicrobial polymer solution. Biofilm formation was evaluated by quantitative analysis using the crystal violet method against *E. Coli* and *S. Aureus* bacteria, which were representatives of Gram-negative and Gram-positive bacteria, respectively. About a 70% reduction in OD600 was achieved with all three coated samples for *S. aureus* compared to the control neat PLA scaffold. Similarly, *E. coli* biofilms were inhibited by 55%, 60%, and 70% on PLA/10/PLA-QAS, PLA/30/PLA-QAS, and PLA/90/PLA-QAS, respectively, compared to the control neat 3D-printed PLA. The impact of the dip-coating technique on mechanical and thermal characteristics was examined, and for both analyses, the plasticizing effect of the coating process with longer dipping times was seen. The flexural strain increased from 0.034 belonging to PLA/10/PLA-QAS to 0.046 belonging to PLA/90/PLA-QAS. It can be said that the mechanical properties of coated materials were not adversely affected after the coating process. As a result of the thermal analysis, a reduction was observed in the  $T_g$  of the

coated samples compared to the neat PLA scaffold. The lowest glass transition temperature was marked as 53 °C for PLA/90/PLA-QAS. These results are correlated with SEM morphologies attributed to the penetration and solution effect of antimicrobial polymer dissolved in acetone. Besides, a cytotoxicity test for all coated samples was performed. It was observed that although all coated samples showed around 20% cell viability in 50% extraction mediums, they were not toxic in 10% and 20% concentrations.

In conclusion, novel 3D-printed PLA materials having anti-biofilm activity were obtained via the dip-coating method. The use of 3D-printed PLA materials that have anti-biofilm properties has the potential to make a substantial difference in various critical medical fields such as surgical instruments, medical implants, wound dressings, catheters, and hospital surfaces. By decreasing the danger of bacterial contamination and biofilm development, these materials can result in better patient outcomes, lower the risk of infections, and aid quicker recovery. Moreover, the antimicrobial agents are attached via covalent bonds and do not leach from the applied surface, and this situation increases its importance in these fields. Also, the application method, dip-coating, is very effective, and it is enough to employ a thin film on the 3D material using a small amount of antimicrobial polymer dissolved in acetone.

**Author contributions:** Conceptualization, FA and GO; methodology, FA and GO; formal analysis, FA; investigation, GU, HB and MC; writing—review and editing, FA, LA and GO; visualization, FA and LA; supervision, GO; project administration, GO; preparation, LA; funding acquisition, GO. All authors have read and agreed to the published version of the manuscript.

**Conflict of interest:** The authors declare no conflict of interest.

## References

1. Water JJ, Bohr A, Boetker J, et al. Three-Dimensional Printing of Drug-Eluting Implants: Preparation of an Antimicrobial Polylactide Feedstock Material. *Journal of Pharmaceutical Sciences*. 2015; 104(3): 1099-1107. doi: 10.1002/jps.24305
2. Muro-Fraguas I, Sainz-García A, López M, et al. Antibiofilm coatings through atmospheric pressure plasma for 3D printed surgical instruments. *Surface and Coatings Technology*. 2020; 399: 126163. doi: 10.1016/j.surfcoat.2020.126163
3. Castro JD, Carneiro E, Marques SM, et al. Surface functionalization of 3D printed structures: Aesthetic and antibiofouling properties. *Surface and Coatings Technology*. 2020; 386: 125464. doi: 10.1016/j.surfcoat.2020.125464
4. Zuo M, Pan N, Liu Q, et al. Three-dimensionally printed polylactic acid/cellulose acetate scaffolds with antimicrobial effect. *RSC Advances*. 2020; 10(5): 2952-2958. doi: 10.1039/c9ra08916k
5. Pastor-Artigues MM, Roure-Fernández F, Ayneto-Gubert X, et al. Elastic Asymmetry of PLA Material in FDM-Printed Parts: Considerations Concerning Experimental Characterisation for Use in Numerical Simulations. *Materials*. 2019; 13(1): 15. doi: 10.3390/ma13010015
6. González-Henríquez CM, Sarabia-Vallejos MA, Rodríguez Hernandez J. Antimicrobial Polymers for Additive Manufacturing. *International Journal of Molecular Sciences*. 2019; 20(5): 1210. doi: 10.3390/ijms20051210
7. Otieno DB, Bosire GO, Onyari JM, et al. Comparative analysis of 3D-printed polylactic acid and acrylonitrile butadiene styrene: Experimental and Materials-Studio-based theoretical studies. *Journal of Polymer Research*. 2022; 29(7). doi: 10.1007/s10965-022-03075-6
8. Weisman JA, Nicholson JC, Tappa K, et al. Antibiotic and chemotherapeutic enhanced three-dimensional printer filaments and constructs for biomedical applications. *International Journal of Nanomedicine*. 2015. doi: 10.2147/ijn.s74811

9. Abd El Aal MI, Awd Allah MM, Abd Alaziz SA, et al. Biodegradable 3D printed polylactic acid structures for different engineering applications: effect of infill pattern and density. *Journal of Polymer Research*. 2023; 31(1). doi: 10.1007/s10965-023-03852-x
10. Chen X, Chen G, Wang G, et al. Recent Progress on 3D-Printed Polylactic Acid and Its Applications in Bone Repair. *Advanced Engineering Materials*. 2019; 22(4). doi: 10.1002/adem.201901065
11. Ambrose CG, Clanton TO. Bioabsorbable implants: review of clinical experience in orthopedic surgery. *Ann. Biomed. Eng.* 2004; 32: 171-177. doi: 10.1023/B:ABME.0000007802.59936.fc
12. Kumar B, Castro M, Feller JF. Poly (lactic acid)–multi-wall carbon nanotube conductive biopolymer nanocomposite vapour sensors. *Sensors and Actuators B: Chemical*. 2012; 161(1): 621-628. doi: 10.1016/j.snb.2011.10.077
13. El Habnoui S, Darcos V, Garric X, et al. Mild Methodology for the Versatile Chemical Modification of Polylactide Surfaces: Original Combination of Anionic and Click Chemistry for Biomedical Applications. *Advanced Functional Materials*. 2011; 21(17): 3321-3330. doi: 10.1002/adfm.201100412
14. Rasal RM, Janorkar AV, Hirt DE. Poly (lactic acid) modifications. *Progress in Polymer Science*. 2010; 35(3): 338-356. doi: 10.1016/j.progpolymsci.2009.12.003
15. Turalija M, Bischof S, Budimir A, et al. Antimicrobial PLA films from environment friendly additives. *Composites Part B: Engineering*. 2016; 102: 94-99. doi: 10.1016/j.compositesb.2016.07.017
16. Chen CH, Yao YY, Tang HC, et al. Long-term antibacterial performances of biodegradable polylactic acid materials with direct absorption of antibiotic agents. *RSC Advances*. 2018; 8(29): 16223-16231. doi: 10.1039/c8ra00504d
17. Popelka A, Abdulkareem A, Mahmoud AA, et al. Antimicrobial modification of PLA scaffolds with ascorbic and fumaric acids via plasma treatment. *Surface and Coatings Technology*. 2020; 400: 126216. doi: 10.1016/j.surfcoat.2020.126216
18. Rodríguez-Contreras A, Torres D, Rafik B, et al. Bioactivity and antibacterial properties of calcium- and silver-doped coatings on 3D printed titanium scaffolds. *Surface and Coatings Technology*. 2021; 421: 127476. doi: 10.1016/j.surfcoat.2021.127476
19. Anthierens T, Billiet L, Devlieghere F, et al. Poly (butylene adipate) functionalized with quaternary phosphonium groups as potential antimicrobial packaging material. *Innovative Food Science & Emerging Technologies*. 2012; 15: 81-85. doi: 10.1016/j.ifset.2012.02.010
20. Tan L, Maji S, Mattheis C, et al. Antimicrobial Hydantoin-grafted Poly( $\epsilon$ -caprolactone) by Ring-opening Polymerization and Click Chemistry. *Macromolecular Bioscience*. 2012; 12(12): 1721-1730. doi: 10.1002/mabi.201200238
21. El Habnoui S, Lavigne JP, Darcos V, et al. Toward potent antibiofilm degradable medical devices: A generic method for the antibacterial surface modification of polylactide. *Acta Biomaterialia*. 2013; 9(8): 7709-7718. doi: 10.1016/j.actbio.2013.04.018
22. Uner A, Doganci E, Tasdelen MA. Non-covalent interactions of pyrene end-labeled star poly( $\epsilon$ -caprolactone)s with fullerene. *Journal of Applied Polymer Science*. 2018; 135(29). doi: 10.1002/app.46520
23. He W, Zhang Y, Li J, et al. A Novel Surface Structure Consisting of Contact-active Antibacterial Upper-layer and Antifouling Sub-layer Derived from Gemini Quaternary Ammonium Salt Polyurethanes. *Scientific Reports*. 2016; 6(1). doi: 10.1038/srep32140
24. Vidakis N, Petousis M, Velidakis E, et al. Three-Dimensional Printed Antimicrobial Objects of Polylactic Acid (PLA)-Silver Nanoparticle Nanocomposite Filaments Produced by an In-Situ Reduction Reactive Melt Mixing Process. *Biomimetics*. 2020; 5(3): 42. doi: 10.3390/biomimetics5030042
25. Venkatesan J, Kim SK, Shim M. Antimicrobial, Antioxidant, and Anticancer Activities of Biosynthesized Silver Nanoparticles Using Marine Algae *Ecklonia cava*. *Nanomaterials*. 2016; 6(12): 235. doi: 10.3390/nano6120235
26. Zhang Q, Zhai W, Cui L, et al. Physicochemical properties and antibacterial activity of polylactic acid/starch acetate films incorporated with chitosan and tea polyphenols. *Polymer Bulletin*. 2023; 80(12): 13319-13341. doi: 10.1007/s00289-023-04691-y
27. Jeong SH, Hwang YH, Yi SC. Antibacterial properties of padded PP/PE nonwovens incorporating nano-sized silver colloids. *Journal of Materials Science*. 2005; 40(20): 5413-5418. doi: 10.1007/s10853-005-4340-2
28. Perelshtein I, Applerot G, Perkas N, et al. Sonochemical coating of silver nanoparticles on textile fabrics (nylon, polyester and cotton) and their antibacterial activity. *Nanotechnology*. 2008; 19(24): 245705. doi: 10.1088/0957-4484/19/24/245705

29. Saini S, Belgacem MN, Missoum K, et al. Natural active molecule chemical grafting on the surface of microfibrillated cellulose for fabrication of contact active antimicrobial surfaces. *Industrial Crops and Products*. 2015; 78: 82-90. doi: 10.1016/j.indcrop.2015.10.022
30. Shi R, Geng H, Gong M, et al. Long-acting and broad-spectrum antimicrobial electrospun poly ( $\epsilon$ -caprolactone)/gelatin micro/nanofibers for wound dressing. *Journal of Colloid and Interface Science*. 2018; 509: 275-284. doi: 10.1016/j.jcis.2017.08.092
31. Saini S, Belgacem MN, Bras J. Effect of variable aminoalkyl chains on chemical grafting of cellulose nanofiber and their antimicrobial activity. *Materials Science and Engineering: C*. 2017; 75: 760-768. doi: 10.1016/j.msec.2017.02.062
32. Muñoz-Bonilla A, Fernández-García M. The roadmap of antimicrobial polymeric materials in macromolecular nanotechnology. *European Polymer Journal*. 2015; 65: 46-62. doi: 10.1016/j.eurpolymj.2015.01.030
33. Tian F, Decker EA, Goddard JM. Controlling lipid oxidation of food by active packaging technologies. *Food & Function*. 2013; 4(5): 669. doi: 10.1039/c3fo30360h
34. Cuervo-Rodríguez R, Muñoz-Bonilla A, Araujo J, et al. Influence of side chain structure on the thermal and antimicrobial properties of cationic methacrylic polymers. *European Polymer Journal*. 2019; 117: 86-93. doi: 10.1016/j.eurpolymj.2019.05.008
35. Dizman B, Elasri MO, Mathias LJ. Synthesis and antimicrobial activities of new water-soluble bis-quaternary ammonium methacrylate polymers. *Journal of Applied Polymer Science*. 2004; 94(2): 635-642. doi: 10.1002/app.20872
36. Bruna JE, Quilodrán H, Guarda A, et al. Development of Antibacterial MtCu/PLA Nanocomposites by Casting Method for Potential Use in Food Packaging. *Journal of the Chilean Chemical Society*. 2015; 60(3): 3009-3014. doi: 10.4067/s0717-97072015000300007
37. Gherasim O, Popescu RC, Grumezescu V, et al. MAPLE Coatings Embedded with Essential Oil-Conjugated Magnetite for Anti-Biofilm Applications. *Materials*. 2021; 14(7): 1612. doi: 10.3390/ma14071612
38. Menon A, Durairajan R, Durai R, et al. Exploration of 3D Printing of Anti-Infective Urinary Catheters: Materials and Approaches to Combat Catheter-Associated Urinary Tract Infections (CAUTIs) - A Review. *Critical Reviews™ in Therapeutic Drug Carrier Systems*. 2022; 39(5): 51-82. doi: 10.1615/critrevtherdrugcarriersyst.2022040452
39. Sandler N, Salmela I, Fallarero A, et al. Towards fabrication of 3D printed medical devices to prevent biofilm formation. *International Journal of Pharmaceutics*. 2014; 459(1-2): 62-64. doi: 10.1016/j.ijpharm.2013.11.001
40. Wang Y, Jayan G, Patwardhan D, Phillips KS. Chapter: Antimicrobial and anti-biofilm medical devices: public health and regulatory science challenges. *Antimicrobial coatings and modifications on medical devices*; 2017.
41. Shenzhen Esun Industrial Co., Ltd. Professional in 3D printing materials. Available online: <https://www.esun3d.com/> (accessed on 7 February 2024).
42. Aynali F, Doganci E, Doruk T, et al. Synthesis and characterization of antimicrobial polylactide via ring-opening polymerization and click chemistry methods. *Polymer International*. 2018; 68(3): 385-393. doi: 10.1002/pi.5721
43. Forster AM. *Materials Testing Standards for Additive Manufacturing of Polymer Materials: State of the Art and Standards Applicability*. National Institute of Standards and Technology; 2015. doi: 10.6028/nist.ir.8059
44. Alharbi HF, Luqman M, Khan ST. Antibiofilm activity of synthesized electrospun core-shell nanofiber composites of PLA and PVA with silver nanoparticles. *Materials Research Express*. 2018; 5(9): 095001. doi: 10.1088/2053-1591/aad4df
45. Liao Y, Xu Q, Zhang J, et al. Cellular response of chondrocytes to magnesium alloys for orthopedic applications. *International Journal of Molecular Medicine*. 2015; 36(1): 73-82. doi: 10.3892/ijmm.2015.2211
46. Feoktistova M, Geserick P, Leverkus M. Crystal Violet Assay for Determining Viability of Cultured Cells. *Cold Spring Harbor Protocols*. 2016; 2016(4): pdb.prot087379. doi: 10.1101/pdb.prot087379
47. Pop MA, Croitoru C, Bedo T, et al. Influence of Internal Innovative Architecture on the Mechanical Properties of 3D Polymer Printed Parts. *Polymers*. 2020; 12(5): 1129. doi: 10.3390/polym12051129